Spin asymmetry A_1^d and the spin-dependent structure function g_1^d of the deuteron at low values of x and Q^2

The COMPASS Collaboration

Abstract

We present a precise measurement of the deuteron longitudinal spin asymmetry A_1^d and of the deuteron spin-dependent structure function g_1^d at $Q^2 < 1$ $(\mathrm{GeV}/c)^2$ and $4 \cdot 10^{-5} < x < 2.5 \cdot 10^{-2}$ based on the data collected by the COMPASS experiment at CERN during the years 2002 and 2003. The statistical precision is tenfold better than that of the previous measurement in this region. The measured A_1^d and g_1^d are found to be consistent with zero in the whole range of x.

The COMPASS Collaboration

E.S. Ageev[24], V.Yu. Alexakhin[8], Yu. Alexandrov[18], G.D. Alexeev[8], A. Amoroso[29],
B. Badełek[30], F. Balestra[29], J. Ball[25], G. Baum[1], Y. Bedfer[25], P. Berglund[13],
C. Bernet[25], R. Bertini[29], R. Birsa[28], J. Bisplinghoff[3], P. Bordalo[15,a],
F. Bradamante[28], A. Bravar[16], A. Bressan[28], E. Burtin[25], M.P. Bussa[29],
V.N. Bytchkov[8], L. Cerini[28], A. Chapiro[27], A. Cicuttin[27], M. Colantoni[29,b],
A.A. Colavita[27], S. Costa[29], M.L. Crespo[27], N. d'Hose[25], S. Dalla Torre[28],
S.S. Dasgupta[6], R. De Masi[20], N. Dedek[19], O.Yu. Denisov[29,c], L. Dhara[7], V. Diaz
Kavka[27], A.M. Dinkelbach[20], A.V. Dolgopolov[24], S.V. Donskov[24], V.A. Dorofeev[24],
N. Doshita[21], V. Duic[28], W. Dünnweber[19], J. Ehlers[12,16], P.D. Eversheim[3],
W. Eyrich[9], M. Fabro[28], M. Faessler[19], V. Falaleev[11], P. Fauland[1], A. Ferrero[29],
L. Ferrero[29], M. Finger[22], M. Finger jr.[8], H. Fischer[10], J. Franz[10], J.M. Friedrich[20],
V. Frolov[29,c], U. Fuchs[11], R. Garfagnini[29], F. Gautheron[1], O.P. Gavrichtchouk[8],
S. Gerassimov[18,20], R. Geyer[19], M. Giorgi[28], B. Gobbo[28], S. Goertz[2,4], A.M. Gorin[24],
O.A. Grajek[30], A. Grasso[29], B. Grube[20], A. Grünemaier[10], J. Hannappel[4], D. von
Harrach[16], T. Hasegawa[17], S. Hedicke[10], F.H. Heinsius[10], R. Hermann[16], C. Heß[2],
F. Hinterberger[3], M. von Hodenberg[10], N. Horikawa[21,d], S. Horikawa[21],
R.B. Ijaduola[27], C. Ilgner[19], A.I. Ioukaev[8], S. Ishimoto[21], O. Ivanov[8], T. Iwata[21,e],
R. Jahn[3], A. Janata[8], R. Joosten[3], N.I. Jouravlev[8], E. Kabuß[16], V. Kalinnikov[28],
D. Kang[10], F. Karstens[10], W. Kastaun[10], B. Ketzer[20], G.V. Khaustov[24],
Yu.A. Khokhlov[24], N.V. Khomutov[8], Yu. Kisselev[1,2], F. Klein[4], S. Koblitz[16],
J.H. Koivuniemi[13], V.N. Kolosov[24], E.V. Komissarov[8], K. Kondo[21],
K. Königsmann[10], A.K. Konoplyannikov[24], I. Konorov[18,20], V.F. Konstantinov[24],
A.S. Korentchenko[8], A. Korzenev[16,c], A.M. Kotzinian[8,29], N.A. Koutchinski[8],
K. Kowalik[30], N.P. Kravchuk[8], G.V. Krivokhizhin[8], Z.V. Kroumchtein[8], R. Kuhn[20],
F. Kunne[25], K. Kurek[30], M.E. Ladygin[24], M. Lamanna[11,28], J.M. Le Goff[25],
M. Leberig[11,16], J. Lichtenstadt[26], T. Liska[23], I. Ludwig[10], A. Maggiora[29],
M. Maggiora[29], A. Magnon[25], G.K. Mallot[11], I.V. Manuilov[24], C. Marchand[25],
J. Marroncle[25], A. Martin[28], J. Marzec[31], T. Matsuda[17], A.N. Maximov[8],
K.S. Medved[8], W. Meyer[2], A. Mielech[28,30], Yu.V. Mikhailov[24], M.A. Moinester[26],
O. Nähle[3], J. Nassalski[30], S. Neliba[23], D.P. Neyret[25], V.I. Nikolaenko[24],
A.A. Nozdrin[8], V.F. Obraztsov[24], A.G. Olshevsky[8], M. Ostrick[4], A. Padee[31],
P. Pagano[28], S. Panebianco[25], D. Panzieri[29,b], S. Paul[20], H.D. Pereira[10,25],
D.V. Peshekhonov[8], V.D. Peshekhonov[8], G. Piragino[29], S. Platchkov[25], K. Platzer[19],
J. Pochodzalla[16], V.A. Polyakov[24], A.A. Popov[8], J. Pretz[4], C. Quintans[15],
S. Ramos[15,a], P.C. Rebourgeard[25], G. Reicherz[2], J. Reymann[10], K. Rith[9,11],
A.M. Rozhdestvensky[8], E. Rondio[30], A.B. Sadovski[8], E. Saller[8], V.D. Samoylenko[24],
A. Sandacz[30], M. Sans[19], M.G. Sapozhnikov[8], I.A. Savin[8], P. Schiavon[28], C. Schill[10],
T. Schmidt[10], H. Schmitt[10], L. Schmitt[20], O.Yu. Shevchenko[8], A.A. Shishkin[8],
H.-W. Siebert[12,16], L. Sinha[7], A.N. Sissakian[8], A. Skachkova[29], M. Slunecka[8],
G.I. Smirnov[8], F. Sozzi[28], V.P. Sugonyaev[24], A. Srnka[5], F. Stinzing[9], M. Stolarski[30],
M. Sulc[14], R. Sulej[31], N. Takabayashi[21], V.V. Tchalishev[8], F. Tessarotto[28],
A. Teufel[9], D. Thers[25], L.G. Tkatchev[8], T. Toeda[21], V.I. Tretyak[8], S. Trousov[8],
M. Varanda[15], M. Virius[23], N.V. Vlassov[8], M. Wagner[9], R. Webb[9], E. Weise[3],
Q. Weitzel[20], U. Wiedner[19], M. Wiesmann[20], R. Windmolders[4], S. Wirth[9],
W. Wiślicki[30], A.M. Zanetti[28], K. Zaremba[31], J. Zhao[16], R. Ziegler[3], and
A. Zvyagin[19]

[1] Universität Bielefeld, Fakultät für Physik, 33501 Bielefeld, Germany[f]

[2] Universität Bochum, Institut für Experimentalphysik, 44780 Bochum, Germany[f]

[3] Universität Bonn, Helmholtz-Institut für Strahlen- und Kernphysik, 53115 Bonn, Germany[f]

[4] Universität Bonn, Physikalisches Institut, 53115 Bonn, Germany[f]

[5] Institute of Scientific Instruments, AS CR, 61264 Brno, Czech Republic[g]

[6] Burdwan University, Burdwan 713104, India[i]

[7] Matrivani Institute of Experimental Research & Education, Calcutta-700 030, India[j]

[8] Joint Institute for Nuclear Research, 141980 Dubna, Moscow region, Russia

[9] Universität Erlangen–Nürnberg, Physikalisches Institut, 91054 Erlangen, Germany[f]

[10] Universität Freiburg, Physikalisches Institut, 79104 Freiburg, Germany[f]

[11] CERN, 1211 Geneva 23, Switzerland

[12] Universität Heidelberg, Physikalisches Institut, 69120 Heidelberg, Germany[f]

[13] Helsinki University of Technology, Low Temperature Laboratory, 02015 HUT, Finland and University of Helsinki, Helsinki Institute of Physics, 00014 Helsinki, Finland

[14] Technical University in Liberec, 46117 Liberec, Czech Republic[g]

[15] LIP, 1000-149 Lisbon, Portugal[h]

[16] Universität Mainz, Institut für Kernphysik, 55099 Mainz, Germany[f]

[17] University of Miyazaki, Miyazaki 889-2192, Japan[k]

[18] Lebedev Physical Institute, 119991 Moscow, Russia

[19] Ludwig-Maximilians-Universität München, Department für Physik, 80799 Munich, Germany[f]

[20] Technische Universität München, Physik Department, 85748 Garching, Germany[f]

[21] Nagoya University, 464 Nagoya, Japan[k]

[22] Charles University, Faculty of Mathematics and Physics, 18000 Prague, Czech Republic[g]

[23] Czech Technical University in Prague, 16636 Prague, Czech Republic[g]

[24] State Research Center of the Russian Federation, Institute for High Energy Physics, 142281 Protvino, Russia

[25] CEA DAPNIA/SPhN Saclay, 91191 Gif-sur-Yvette, France

[26] Tel Aviv University, School of Physics and Astronomy, 69978 Tel Aviv, Israel[l]

[27] ICTP–INFN MLab Laboratory, 34014 Trieste, Italy

[28] INFN Trieste and University of Trieste, Department of Physics, 34127 Trieste, Italy

[29] INFN Turin and University of Turin, Physics Department, 10125 Turin, Italy

[30] Sołtan Institute for Nuclear Studies and Warsaw University, 00-681 Warsaw, Poland[m]

[31] Warsaw University of Technology, Institute of Radioelectronics, 00-665 Warsaw, Poland[n]

[a] Also at IST, Universidade Técnica de Lisboa, Lisbon, Portugal

[b] Also at University of East Piedmont, 15100 Alessandria, Italy

[c] On leave of absence from JINR Dubna

[d] Also at Chubu University, Kasugai, Aichi, 487-8501 Japan

[e] Also at Yamagata University, Yamagata, 992-8510 Japan

In the nucleon structure investigations by high energy lepton probes, the region of low x corresponds to high parton densities, where new dynamical mechanisms may be revealed. The longitudinal structure function $g_1(x, Q^2)$ is presently the only observable which permits the study of low x processes in spin dependent interactions. The existing data have been obtained exclusively from fixed-target experiments where the low values of x strongly correlate with low values of Q^2. Therefore theoretical interpretations of the results require a suitable extrapolation of the parton ansatz to the low-Q^2 region and possibly also an inclusion of nonperturbative mechanisms, which vanish at higher Q^2.

Contrary to the spin-independent structure functions, the small-x behaviour of both the singlet and the non-singlet part of g_1 is controlled by double logarithmic terms, *i.e.* by those terms which correspond to powers of $\ln^2(1/x)$ at each order of the perturbative expansion [1]. The double logarithmic effects go beyond the DGLAP evolution and can be accommodated in it using special techniques [2–4]. Different approaches permit a smooth extrapolation of the obtained g_1 to the low-Q^2 region [4,5] where it may also be complemented by a non-perturbative component [6]. The double logarithmic terms generate the leading small-x behaviour of g_1 where the relevant Regge poles are expected to have a low intercept.

The region of low x and fixed Q^2 is the Regge limit of the (deep) inelastic scattering where the Regge pole exchange model should be applicable. In this model the shape of g_1 at $x \to 0$ (*i.e.* at $Q^2 \ll W^2$ where W^2 is the $\gamma^* N$ centre-of-mass energy squared) is parametrised as

$$g_1^i(x, Q^2) \sim \beta(Q^2) x^{-\alpha_i(0)}. \tag{1}$$

Here the index i refers to the flavour singlet (s) and nonsinglet (ns) combinations of proton and neutron structure functions and $\alpha_i(0)$ denotes the Regge trajectory function at zero momentum transfer. It is expected that $\alpha_{s,ns}(0) \lesssim 0$ and that $\alpha_s(0) \approx \alpha_{ns}(0)$ [7]. This behaviour of g_1 should translate to the $W^{2\alpha}$ dependence of the Compton cross-section at $Q^2 \to 0$ where g_1 should be a finite function of W^2, free from any kinematical singularities or zeros.

The spin-dependent structure function of the deuteron $g_1^d(x, Q^2)$ has been accurately measured in the perturbative region, $Q^2 > 1$ $(\text{GeV}/c)^2$ [8–12]. Due to the relatively low incident energy, the deep inelastic scattering events collected in those experiments cover only a limited range of x. The behaviour of g_1 at $x \lesssim 0.001$ in the large-Q^2 region is unknown due to the lack of data from colliders with polarised beams.

Measurements at low x and low Q^2 put very high demands on event triggering and reconstruction and are very scarce: they were performed only by the SMC at CERN on proton and deuteron targets [13]. Here we present new results from the COMPASS experiment at CERN on the deuteron longitudinal spin asymmetry A_1^d and the spin-dependent structure function g_1^d in the range $0.001 < Q^2 < 1$ $(\text{GeV}/c)^2$ in the photon virtuality and $4 \cdot 10^{-5} < x < 2.5 \cdot 10^{-2}$ in the Bjorken scaling variable. This range is essentially the same as that covered by the SMC [13], but the present measurements result in about tenfold better precision. They complement our recently published measurements obtained in the region $0.004 < x < 0.7$ and $1 < Q^2 < 100$ $(\text{GeV}/c)^2$ [12]. The data were collected during the years 2002 and 2003. They cover the kinematic range presented in Fig. 1. We refer the reader to reference [14] for the description of the 160 GeV/c positive muon beam, the two-cell ^{6}LiD polarised target and the COMPASS spectrometer and to Ref. [15] for a detailed description of the analysis.

The COMPASS data acquisition system is triggered by coincidence signals in ho-

doscopes, defining the direction of the scattered muon behind the spectrometer magnets and/or by a signal in the hadron calorimeters [16]. Triggers due to halo muons are suppressed by veto counters installed upstream of the target. COMPASS uses three types of triggers: i) inclusive ones, based on muon detection only ii) semi-inclusive triggers, based on muon detection and presence of energy deposit in the hadron calorimeters and iii) a calorimetric trigger where only information from the hadron calorimeters is used. The low-x and low-Q^2 region is dominated by semi-inclusive triggers. The contribution of the inclusive ones is below 5% for $x < 0.001$ and exceeds 30% only for $x > 0.01$. Also the contribution of the standalone calorimetric trigger is negligible there. In the kinematic region considered here events are characterised by small muon scattering angles and their kinematics may be distorted by real photon emission. Therefore in the analysis presented here the so-called hadron method [8] is used. This means that all events in our sample require the presence of the trajectories of a reconstructed beam muon, a scattered muon and at least one additional outgoing particle, together defining an interaction point. The presence of hadrons in the final state improves the reconstruction of the interaction point and reduces the background of events originating from radiative processes and from the muons scattered off atomic electrons. It has been checked that the use of the hadron method does not bias the inclusive asymmetries [8].

The momentum of the incoming muon, centred around 160 GeV/c and measured in the beam spectrometer, is required to be between 140 and 180 GeV/c. The reconstructed interaction point has to be located inside one of the target cells. In addition, the extrapolated beam muon trajectory is required to cross entirely both target cells in order to equalize the flux seen by each of them. The scattered muon is identified by detectors situated behind hadron absorbers and its trajectory must be consistent with the hodoscope signals used for the event trigger.

Events are selected by cuts on the four-momentum transfer squared, $Q^2 < 1\,(\text{GeV}/c)^2$, the fractional energy of the virtual photon, $0.1 < y < 0.9$, and the scaling variable $x > 4 \cdot 10^{-5}$. The remaining cuts are the same as those used in the $Q^2 > 1\,(\text{GeV}/c)^2$ analysis [12], with additional quality checks on the interaction point, appropriate to the present kinematics [15]. According to the hadron method we also require the most energetic hadron having $z_h > 0.1$ (z_h is a fraction of the virtual photon energy in the laboratory frame, carried by a hadron).

At low values of x the sample is contaminated by events of muon elastic scattering off atomic electrons, $\mu^+ e^- \rightarrow \mu^+ e^-$, occurring at $x_{\mu e} = m_{\text{electron}}/M = 5.45 \cdot 10^{-4}$ (M is the proton mass) and at very small scattering angles. To remove such events, cuts are imposed on a variable, $q\theta$, defined as the product of the angle θ between the virtual photon and the hadron candidate and the sign q of the electric charge of the hadron. Depending upon the number of hadron candidates outgoing from the interaction point, the event is rejected if $-5 < q\theta < 2$ mrad or $-2 < q\theta < 0$ mrad depending whether it contains one or two hadron candidates [1]. The distribution of the $q\theta$ variable and the x spectrum before and after the μe scattering rejection are presented in Fig. 2. The background of μe events which remains under the elastic peak is estimated to be smaller than 1% of the data sample. As the electromagnetic calorimeter (ECAL) could not be fully used in the present analysis, the cuts used for μe scattering rejection presented above are applied in the whole range of x to reduce the yield of unwanted radiative events. A study using a small subsample of events where the ECAL was available shows that around 50% of those unwanted events

---

[1] A part of that condition, $0 < q\theta < 2$ mrad, encompasses misidentified muons and beam halo muons.

are excluded from the data sample in this way. The remaining background of radiative events accounts for less than about 1% of the data sample.

During data taking the two target cells are polarised in opposite directions, so that the deuteron spins are parallel or antiparallel to the spins of the incoming muons. The spins are inverted every 8 hours by a rotation of the target magnetic field. In 2002 and 2003 the average beam and target deuteron polarisations were about -0.76 and ± 0.51, respectively.

Extraction of the cross-section asymmetry A_1^d in the kinematic region where Q^2 extends down to about 0.001 $(\text{GeV}/c)^2$ demands special care. The common practise of neglecting the m_μ^2/Q^2 terms (m_μ is the muon mass) in the expression for the cross-sections cannot be applied in this region. Therefore we present below the general spin formalism where all the m_μ^2/Q^2 terms are properly taken into account. The only approximation applied is neglecting the m_μ^2/E^2 terms (E is the incident muon energy) which are of the order of 10^{-7} at our kinematics. In all the formulae we consider the exchange of one virtual photon only. The interference effects between virtual Z^0 and photon exchange in the inelastic muon scattering have been measured in an unpolarised experiment [17] and found negligible in the kinematic range of current fixed target experiments (see also [18]).

The polarised inelastic muon–deuteron inclusive scattering cross-section σ in the one-photon exchange approximation can be written as the sum of a spin-independent term $\bar{\sigma}$ and a spin-dependent term $\Delta\sigma$ and involves the muon helicity $h_\mu = \pm 1$

$$\sigma = \bar{\sigma} - \frac{1}{2} h_\mu \Delta\sigma. \tag{2}$$

Eight independent structure functions parametrise the cross-section for a spin-1 target; this is twice as many as for the spin-1/2 case. Apart of the spin-independent structure functions F_1 and F_2 and the spin-dependent structure functions g_1 and g_2, four additional structure functions, b_1, b_2, b_3, b_4 are needed in the spin-1 case [19]. All these functions depend on Q^2 and x. Following previous analyses, cf. Refs. [8,12,13] we neglect b_{1-4} since they are predicted to be small [19]. Then the expressions for the cross-sections $\bar{\sigma}$ and $\Delta\sigma$ and thus the cross-section asymmetries $A_\parallel$ and $A_\perp$ become identical to those for a spin-1/2 target.

The spin-independent cross-section for parity-conserving interactions can be expressed in terms of two unpolarized structure functions F_1 and F_2:

$$\bar{\sigma} \equiv \frac{\mathrm{d}^2\bar{\sigma}}{\mathrm{d}x\mathrm{d}Q^2} = \frac{4\pi\alpha^2}{Q^4 x}\left[xy^2\left(1 - \frac{2m_\mu^2}{Q^2}\right)F_1(x, Q^2) + \left(1 - y - \frac{\gamma^2 y^2}{4}\right)F_2(x, Q^2)\right], \tag{3}$$

where

$$\gamma = \frac{2Mx}{\sqrt{Q^2}} = \frac{\sqrt{Q^2}}{\nu} \tag{4}$$

and ν is the energy of the exchanged virtual photon.

When the muon spin and the deuteron spin form an angle ψ, the cross-section $\Delta\sigma$ can be expressed as [20]

$$\Delta\sigma = \cos\psi\,\Delta\sigma_\parallel + \sin\psi\,\cos\phi\,\Delta\sigma_\perp. \tag{5}$$

3

Here ϕ is the azimuthal angle between the scattering plane and the spin plane. The cross-sections $\Delta\sigma_\parallel$ and $\Delta\sigma_\perp$ refer to the two configurations where the deuteron spin is (anti)parallel or orthogonal to the muon spin; $\Delta\sigma_\parallel$ is the difference between the cross-sections for antiparallel and parallel spin orientations and $\Delta\sigma_\perp = \Delta\sigma_T/\cos\phi$, the difference between the cross-sections at angles ϕ and $\phi + \pi$. The corresponding differential cross-sections, which can be written in terms of the two structure functions g_1 and g_2, are given by

$$\Delta\sigma_\parallel \equiv \frac{\mathrm{d}^2\Delta\sigma_\parallel}{\mathrm{d}x\mathrm{d}Q^2} = \frac{16\pi\alpha^2 y}{Q^4}\left[\left(1 - \frac{y}{2} - \frac{\gamma^2 y^2}{4} - \frac{m_\mu^2 y^2}{Q^2}\right)g_1 - \frac{\gamma^2 y}{2}g_2\right] \tag{6}$$

and

$$\Delta\sigma_T = \cos\phi\Delta\sigma_\perp \equiv \frac{\mathrm{d}^3\Delta\sigma_T}{\mathrm{d}x\mathrm{d}Q^2\mathrm{d}\phi} = \cos\phi \frac{8\alpha^2 y}{Q^4}\gamma\sqrt{1 - y - \frac{\gamma^2 y^2}{4}}\left[\frac{y}{2}\left(1 + \frac{2m_\mu^2}{Q^2}y\right)g_1 + g_2\right]. \tag{7}$$

The relevant asymmetries are

$$A_\parallel = \frac{\Delta\sigma_\parallel}{2\bar{\sigma}}, \qquad A_\perp = \frac{\Delta\sigma_\perp}{2\bar{\sigma}}. \tag{8}$$

The cross-section asymmetry $A_\parallel^d = (\sigma^{\uparrow\downarrow} - \sigma^{\uparrow\uparrow})/(\sigma^{\uparrow\downarrow} + \sigma^{\uparrow\uparrow})$, for antiparallel ($\uparrow\downarrow$) and parallel ($\uparrow\uparrow$) spins of the incoming muon and the target deuteron can be obtained from the numbers of events N_i collected from each cell before and after reversal of the target spins:

$$N_i = a_i\phi_i n_i\bar{\sigma}(1 + P_B P_T f A_\parallel^d), \qquad i = 1, 2, 3, 4, \tag{9}$$

where a_i is the acceptance, ϕ_i the incoming flux, n_i the number of target nucleons, P_B and P_T the beam and target polarisations and f the effective target dilution factor. The latter includes a corrective factor $\rho = \sigma_d^{1\gamma}/\sigma_d^{tot}$ [21] accounting for radiative events on the unpolarised deuteron and a correction for the relative polarisation of deuterons bound in ^{6}Li compared to free deuterons. Average values of f in bins of x for the final data sample are presented in Fig. 4. The extraction of the spin asymmetry was performed as in Refs. [12,22]. The four relations of Eq. (9), corresponding to the two cells and two spin orientations, lead to a second-order equation in $A_\parallel^d$. This method ensures that fluxes and acceptances cancel out in the asymmetry calculation on the condition that the ratio of the acceptances of the two cells is the same before and after spin reversal, cf. Ref. [18].

The longitudinal and transverse virtual-photon deuteron asymmetries, A_1^d and A_2^d, are defined via the asymmetry of absorption cross-sections of transversely polarised photon as

$$A_1^d = (\sigma_0^T - \sigma_2^T)/(2\sigma^T), \qquad A_2^d = (\sigma_0^{TL} + \sigma_1^{TL})/(2\sigma^T), \tag{10}$$

where σ_J^T is the γ^*-deuteron absorption cross-section for a total spin projection J in the photon direction, σ_J^{TL} results from the interference between transverse and longitudinal amplitudes for $J = 0, 1$ and $\sigma^T = (\sigma_0^T + \sigma_1^T + \sigma_2^T)/3$ is the total transverse photoabsorption cross-section. The relation between A_1^d, A_2^d and the experimentally measured $A_\parallel^d, A_\perp^d$ is

$$A_\parallel^d = D(A_1^d + \eta A_2^d), \qquad A_\perp^d = d(A_2^d - \xi A_1^d), \tag{11}$$

where D (the so called depolarisation factor), η, d and ξ depend on kinematics:

4

$$D = \frac{y\left[(1+\gamma^2 y/2)(2-y) - 2y^2 m_\mu^2/Q^2\right]}{y^2(1-2m_\mu^2/Q^2)(1+\gamma^2) + 2(1+R)(1-y-\gamma^2 y^2/4)}, \tag{12}$$

$$\eta = \frac{\gamma\left(1-y-\gamma^2 y^2/4 - y^2 m_\mu^2/Q^2\right)}{(1+\gamma^2 y/2)(1-y/2) - y^2 m_\mu^2/Q^2}, \tag{13}$$

$$d = \frac{\sqrt{1-y-\gamma^2 y^2/4}\,(1+\gamma^2 y/2)}{(1-y/2)(1+\gamma^2 y/2) - y^2 m_\mu^2/Q^2} D, \tag{14}$$

$$\xi = \frac{\gamma(1-y/2 - y^2 m_\mu^2/Q^2)}{1+\gamma^2 y/2}. \tag{15}$$

In view of the small value of η in our kinematic region the expression for A_1^d in Eq. (11) is reduced to $A_1^d \simeq A_\parallel^d/D$ and the possible contribution from the neglected term is included in the systematic errors [15]. The virtual-photon depolarisation factor D depends on the ratio of longitudinal and transverse photoabsorption cross-sections, $R = \sigma^L/\sigma^T$. In the present analysis an updated parametrisation of R taking into account all existing measurements is used [23] together with an extension to very low values of Q^2, cf. Appendix. Average values of D and R in bins of x are shown in Figs. **??**, respectively.

In order to minimize the statistical error of the asymmetry, the kinematic factors f, D and the beam polarisation P_B are calculated event-by-event and used to weight events. This approach improves the statistical precision by approximately 8% as compared to asymmetry evaluation from events numbers. In the weight calculations a parametrisation of P_B as a function of the beam momentum is used. For P_T an average value is used for the data sample taken between two consecutive target spin reversals [2]. The obtained asymmetry is corrected for spin-dependent radiative effects according to Ref. [24] but retaining only radiative inelastic tails.

The final values of $A_1^d(x, Q^2)$ are listed in Table 1 with the corresponding average values of x and Q^2. They are also shown as a function of x in Fig. 7. These values confirm, with a statistical precision increased by more than an order of magnitude, the observation made in Ref. [13] that the asymmetry is consistent with zero for $x \lesssim 0.01$.

The systematic error of A_1^d contains multiplicative contributions resulting from uncertainties on polarisations P_B and P_T, on the dilution factor f and on the function R used to calculate the depolarisation factor D. Of these, the largest contribution comes from D due to a poor knowledge of R. When combined in quadrature, these errors amount to 10–30% (Table 2). However the most important contribution to the systematic error is due to possible false asymmetries which could be generated by instabilities in some components of the spectrometer. In order to minimize their effect, the values of A_1^d in each interval of x have been calculated for 97 subsamples, each of them covering a short period of running time and, therefore, ensuring similar detector operating conditions. An upper limit of the effect of the time dependent detector instabilities has been evaluated by a statistical approach. Dispersions of the values of A_1^d around their means at each value of x were compared with their expected values. Using the Monte Carlo technique for a statistical limit estimate [25], values for the false asymmetries were calculated and everywhere found to be smaller than the statistical precision. This estimate accounts for the time variation effects of the spectrometer components.

---

[2] As P_T varies with time, using it in the weight would bias the A_1 asymmetry.

Several other searches for false asymmetries were performed. Data from the two target cells were combined in different ways in order to eliminate the spin-dependent asymmetry. Data obtained with opposite signs of cell polarisations were compared as they may reveal acceptance effects. These searches did not show any significant false asymmetry.

In Fig. 8 results of the present analysis as a function of x are presented together with previous measurements by the SMC at $0.01 < Q^2 < 100$ $(\text{GeV}/c)^2$ [8, 13]. The improvement in the statistical precision at low x is striking. Other data, mostly from the deep inelastic scattering region by COMPASS [12], HERMES [11], SLAC E143 [9] and SLAC E155 [10], are also presented in Fig. 8. The values of A_1^d, even if originating from experiments at different energies, tend to coincide due to the very small Q^2 dependence of A_1^d at fixed x.

The spin dependent structure functions are connected to the virtual photon asymmetries in the following way

$$g_1^d = \frac{F_1^d}{(1+\gamma^2)} \left(A_1^d + \gamma A_2^d\right), \qquad g_2^d = \frac{F_1^d}{(1+\gamma^2)} \left(-A_1^d + \frac{1}{\gamma}A_2^d\right). \qquad (16)$$

These formulae are exact; possible contributions from the structure functions b_{1-4} cancel out. Neglecting A_2^d and making the usual replacement $(1+\gamma^2)F_2/(2xF_1) = 1+R$, as in the spin-1/2 case and valid if $b_{1-4} = 0$, the longitudinal spin structure function g_1^d is obtained as

$$g_1^d = \frac{F_2^d}{2\ x\ (1+R)} A_1^d. \qquad (17)$$

The values of g_1^d are listed in the last column of Table 1 and shown in Fig. 9. They have been obtained with the F_2^d parametrisation of Refs. [8, 26], cf. Appendix, and with the parametrisation of R used in the depolarisation factor. The systematic errors on g_1^d are obtained in the same way as for A_1^d, with an additional contribution from the uncertainty on F_2^d. Moreover the error of the depolarisation factor was modified. Instead of δD, the error of the quantity $D(1 + R)$, $\delta[D(1 + R)]$ was considered. The values of $xg_1^d(x)$ obtained in this analysis and, for comparison, the SMC [13] and HERMES [11] results at $Q^2 < 1$ $(\text{GeV}/c)^2$ are shown in Fig. 10.

The low x data in the kinematic region where W^2 is high and $W^2 \gg Q^2$, should in principle allow testing the Regge behaviour of g_1 through its x dependence. These conditions are fulfilled by our measurements and thus a fit of Eq. (1) to the g_1 data from the Q^2 range of $0.0025 - 0.25$ $(\text{GeV}/c)^2$ in six subintervals of $Q^2 \approx$ const was performed. The results of the fit were inconclusive. No information on the singlet intercept, $\alpha_s(0)$, could be extracted. Thus our data do not provide a test of the Regge behaviour of g_1 without additional assumptions about its Q^2 dependence. This is due to a limited x interval for any given value of Q^2 combined with small measured values of g_1^d. However, these data can be compared with models predicting both the x and Q^2 dependence of g_1 at low values of x and Q^2 [4, 6]. A relevant phenomenological analysis is in progress.

In summary, we have measured the deuteron spin asymmetry A_1^d and its longitudinal spin-dependent structure function g_1^d for $Q^2 < 1$ $(\text{GeV}/c)^2$ over the range $4 \cdot 10^{-5} < x < 2.5 \cdot 10^{-2}$ and with a statistical precision more than tenfold better than previous experiments. The A_1^d and g_1^d values are compatible with zero for $x \lesssim 0.01$.

6

Acknowledgements

Appendix

Knowledge of $F_2(x, Q^2)$ and $R(x, Q^2)$ is needed in computations of the dilution factor, the radiative corrections, the depolarisation factor and the spin dependent structure function $g_1(x, Q^2)$. It is not sufficient to know these functions only in the kinematic range of the analysis since radiative corrections require their knowledge at $x > x_{meas}$ and all values of Q^2 including $Q^2 = 0$, due to radiative "tails". Asymptotic behaviours of F_2 and R in the photoproduction limit, $Q^2 \to 0$, are: $F_2 \sim Q^2$ and $R \sim Q^2$ (for fixed, arbitrary ν). These kinematic constraints eliminate potential kinematical singularities at $Q^2 = 0$ of the hadronic tensor defining the virtual Compton scattering amplitude.

In the analysis, a new SLAC parametrisation of R, R_{1998} [23], and F_2 parametrisation of Ref. [8] is employed. The former, valid for $Q^2 > 0.5$ $(\text{GeV}/c)^2$, is extended to lower values of Q^2, including the $R \sim Q^2$ behaviour at $Q^2 = 0$, as:

$$R(Q^2 < 0.5 \ (\text{GeV}/c)^2, x) = R_{1998}(0.5 \ (\text{GeV}/c)^2, x) \cdot \beta(1 - \exp(-Q^2/\alpha)) \qquad (18)$$

with $\alpha = 0.2712$ and $\beta = 1/(1 - \exp(0.5/\alpha)) = 1.1880$. At $Q^2 = 0.5$ $(\text{GeV}/c)^2$ the function and its first derivative are continuous in the whole x range of our measurements. The error on R, δR, above $Q^2 = 0.5$ $(\text{GeV}/c)^2$ was taken from Ref. [23] and below $Q^2 = 0.5$ $(\text{GeV}/c)^2$ was set to 0.2. For this value of δR and for the simplest assumption about R at $Q^2 < 0.5$ $(\text{GeV}/c)^2$ and any x (*e.g.* $R = 0.2$) there is an approximate agreement (within 1σ) with both the value $R = 0$ at the photoproduction limit and with measurements at higher Q^2 from HERA, where $R \approx 0.4$ [27].

The F_2 of Ref. [8] is valid for $Q^2 > 0.2$ $(\text{GeV}/c)^2$ and $x > 0.0009$. At lower values of Q^2 and x we used the model of Ref. [26] valid down to $Q^2 = 0$ and $x = 10^{-5}$ and based on a concept of generalised vector meson dominance. Two other F_2 parametrisations, albeit for the proton [28, 29], were also tried together with Ref. [26], to estimate the F_2 uncertainty, δF_2. The former of these parametrisations is based on the parton saturation model with recent modifications including the QCD evolution and the latter is a Regge motivated fit to all the world data of F_2^p, extended into the large Q^2 in a way compatible with QCD expectations. They are valid in a range similar to that of Ref. [26]. The δF_2 uncertainty was taken as the largest difference between the values of the employed F_2 and other parametrisations.

References

[1] J. Bartels, B.I. Ermolaev and M. G. Ryskin, Z. Phys. C **70** (1996) 273; Z. Phys. C **72** (1996) 627.

[2] J. Blümlein and A. Vogt, Acta Phys. Polon. **B27** (1996) 1309; Phys. Lett. **B386** (1996) 350; J. Blümlein, S. Riemersma and A. Vogt Nucl. Phys. B (Proc. Suppl) **51C** (1996) 30.

[3] J.Kwieciński and B.Ziaja, Phys. Rev. D **60** (1999) 054004.

[4] B.I. Ermolaev, M. Greco and S.I. Troyan, hep-ph/0605133; hep-ph/0607024.

[5] B. Badełek and J. Kwieciński, Phys. Lett. B **418** (1998) 229.

[6] B. Badełek, J. Kwieciński and J. Kiryluk, Phys. Rev. D **61** (2000) 014009; B. Badełek, J. Kwieciński and B. Ziaja, Eur. Phys. J. C **26** (2002) 45.

[7] R.L. Heimann, Nucl. Phys. **B64** (1973) 429; J. Ellis and M. Karliner, Phys. Lett. **B213** (1988) 73; B.L. Ioffe, V.A. Khoze, and L.N. Lipatov, *'Hard Processes'*, (North-Holland, Amsterdam, 1984).

[8] SMC Collaboration, B. Adeva *et al.,* Phys. Rev. D **58** (1998) 112001.

[9] E143 Collaboration, K. Abe *et al.,* Phys. Rev. D **58** (1998) 112003.

[10] E155 Collaboration, P. L. Anthony *et al.,* Phys. Lett. B **463** (1999) 339.

[11] HERMES Collaboration, A. Airapetian *et al.,* preprint DESY/06-142, September 21, 2006.

[12] COMPASS Collaboration, V.Yu. Alexakhin *et al.,* hep-ex/0609038 and submitted to the Phys. Lett. B.

[13] SMC Collaboration, B. Adeva *et al.,* Phys. Rev. D **60** (1999) 072004; erratum *ibid,* D **62** (2000) 079902.

[14] G.K. Mallot, Nucl. Instrum. Methods A **518** (2004) 121.

[15] M. Stolarski, PhD Thesis, Warsaw University, 2006; http://wwwcompass.cern.ch/compass/publications/welcome.html#theses.

[16] C. Bernet *et al.,* Nucl. Instrum. Methods A **550** (2005) 217.

[17] BCDMS Collaboration, A. Argento *et al.,* Phys. Lett. B **120** (1983) 245; *ibid.* **140** (1984) 142.

[18] SMC Collaboration, D. Adams *et al.,* Phys. Rev. D **56** (1997) 5330.

[19] P. Hoodbhoy, R.L. Jaffe and A.V. Manohar, Nucl. Phys. B **312** (1989) 571; H. Khan and P. Hoodbhoy, Phys. Lett. B **298** (1993) 181.

[20] R.L. Jaffe, Comments Nucl. Phys. **19**, 239 (1990).

[21] A. A. Akhundov *et al.*, Fortsch. Phys. **44** (1996) 373.

[22] COMPASS Collaboration, E. S. Ageev *et al.,* Phys. Lett. B **612** (2005) 154.

[23] E143 Collaboration, K. Abe *et al.,* Phys. Lett. B **452** (1999) 194.

[24] I. V. Akushevich and N. M. Shumeiko, J. Phys. G **20** (1994) 513.

[25] O. Helene, Nucl. Instrum. Methods **212** (1983) 319.

[26] J. Kwieciński and B. Badełek, Z. Phys. C **43** (1989) 251; B. Badełek and J. Kwieciński, Phys. Lett. B **295** (1992) 263.

[27] H1 Collaboration, C. Adloff *et al.*, Phys. Lett. B **393** (1997) 452; H1 and ZEUS Collaborations, T. Laštovička, Eur. Phys. J. C **33** (2004) s388.

[28] J. Bartels, K. Golec-Biernat and H. Kowalski, Phys. Rev. D **66** (2002) 014001.

[29] H. Abramowicz and A. Levy, DESY 97–251 and hep-ph/9712415.

x range	$\langle x \rangle$	$\langle Q^2 \rangle$ $[(\mathrm{GeV}/c)^2]$	$\langle y \rangle$	A_1^d	g_1^d
0.000063– 0.00004	0.000052	0.0068	0.44	$0.0008 \pm 0.0036 \pm 0.0034$	$0.06 \pm 0.27 \pm 0.26$
0.00004 – 0.0001	0.000081	0.012	0.49	$-0.0027 \pm 0.0027 \pm 0.0017$	$-0.22 \pm 0.23 \pm 0.14$
0.0001 – 0.00016	0.00013	0.021	0.53	$0.0015 \pm 0.0023 \pm 0.0014$	$0.13 \pm 0.21 \pm 0.12$
0.00016 – 0.00025	0.00020	0.034	0.56	$-0.0007 \pm 0.0022 \pm 0.0015$	$-0.06 \pm 0.19 \pm 0.13$
0.00025 – 0.0004	0.00032	0.054	0.56	$0.0045 \pm 0.0022 \pm 0.0017$	$0.36 \pm 0.18 \pm 0.14$
0.0004 – 0.00063	0.00050	0.085	0.56	$-0.0022 \pm 0.0023 \pm 0.0013$	$-0.16 \pm 0.17 \pm 0.09$
0.00063 – 0.001	0.00079	0.13	0.55	$-0.0005 \pm 0.0025 \pm 0.0015$	$-0.03 \pm 0.16 \pm 0.09$
0.001 – 0.0016	0.0013	0.20	0.54	$-0.0035 \pm 0.0029 \pm 0.0022$	$-0.11 \pm 0.09 \pm 0.09$
0.0016 – 0.0025	0.0020	0.32	0.54	$-0.0023 \pm 0.0035 \pm 0.0025$	$-0.07 \pm 0.10 \pm 0.07$
0.0025 – 0.004	0.0031	0.50	0.53	$-0.0013 \pm 0.0043 \pm 0.0034$	$-0.03 \pm 0.10 \pm 0.08$
0.004 – 0.0063	0.0049	0.63	0.43	$-0.0069 \pm 0.0061 \pm 0.0033$	$-0.11 \pm 0.10 \pm 0.06$
0.0063 – 0.01	0.0077	0.68	0.30	$-0.016 \pm 0.010 \pm 0.008$	$-0.17 \pm 0.11 \pm 0.09$
0.01 – 0.0158	0.012	0.74	0.20	$0.013 \pm 0.019 \pm 0.012$	$0.09 \pm 0.13 \pm 0.09$
0.0158 – 0.025	0.019	0.82	0.14	$0.019 \pm 0.040 \pm 0.019$	$0.09 \pm 0.20 \pm 0.09$

Table 1: Values of A_1^d and g_1^d with their statistical and systematic errors as a function of x with the corresponding average values of x, Q^2 and y. The maximum Q^2 cut is 1 $(\mathrm{GeV}/c)^2$. Bins in x are of equal width in $\log_{10} x$.

Multiplicative variables error	Beam polarisation	$\delta P_B / P_B$	4%
	Target polarisation	$\delta P_T / P_T$	5%
	Depolarisation factor	$\delta D(R) / D(R)$	4 – 30 %
	Dilution factor	$\delta f / f$	7 %
Additive variables error	Transverse asymmetry	$\eta \cdot \delta A_2$	$< 0.1 \cdot \delta A_1^{stat}$
	Radiative corrections	δA_1^{RC}	$< 0.03 \cdot \delta A_1^{stat}$
	False asymmetry	A_{false}	$< \delta A_1^{stat}$

Table 2: Decomposition of the systematic error of A_1 into multiplicative and additive variables contributions.
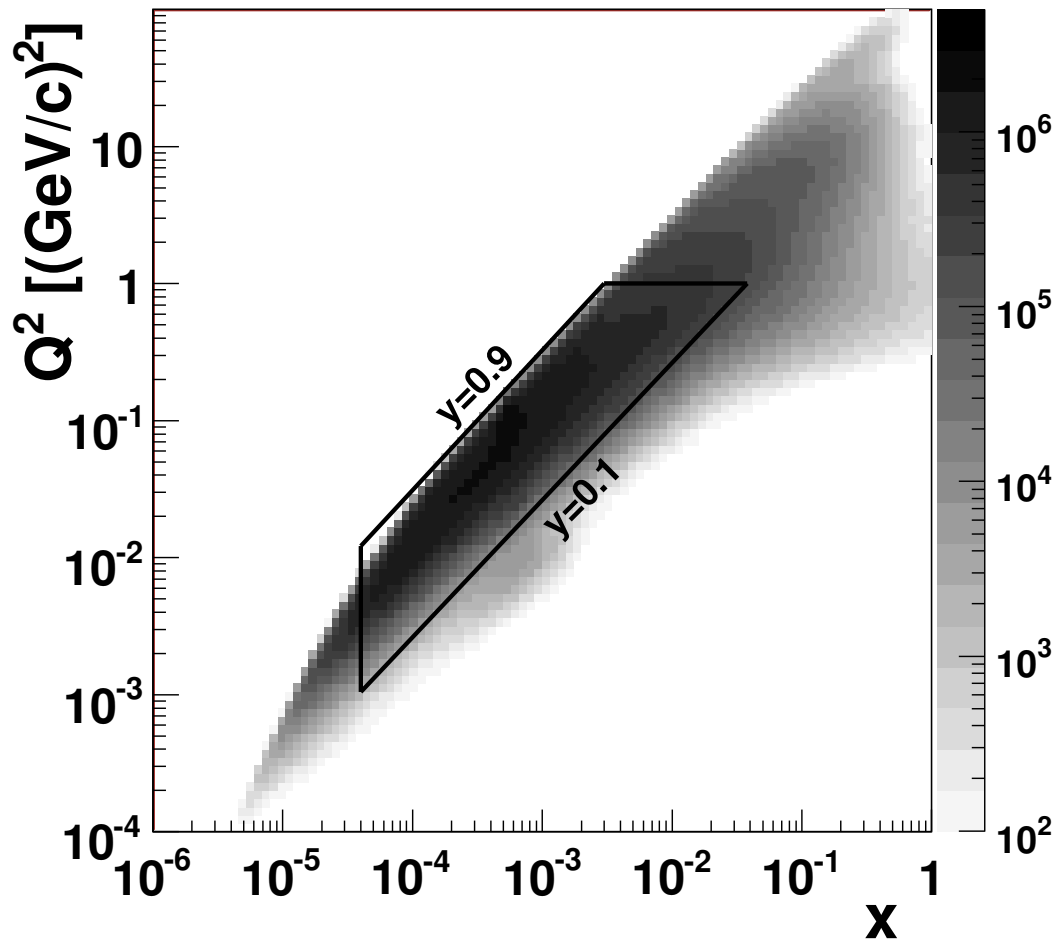
Figure 1: COMPASS acceptance in the (x, Q^2) plane. The contour indicates the region selected for this analysis.
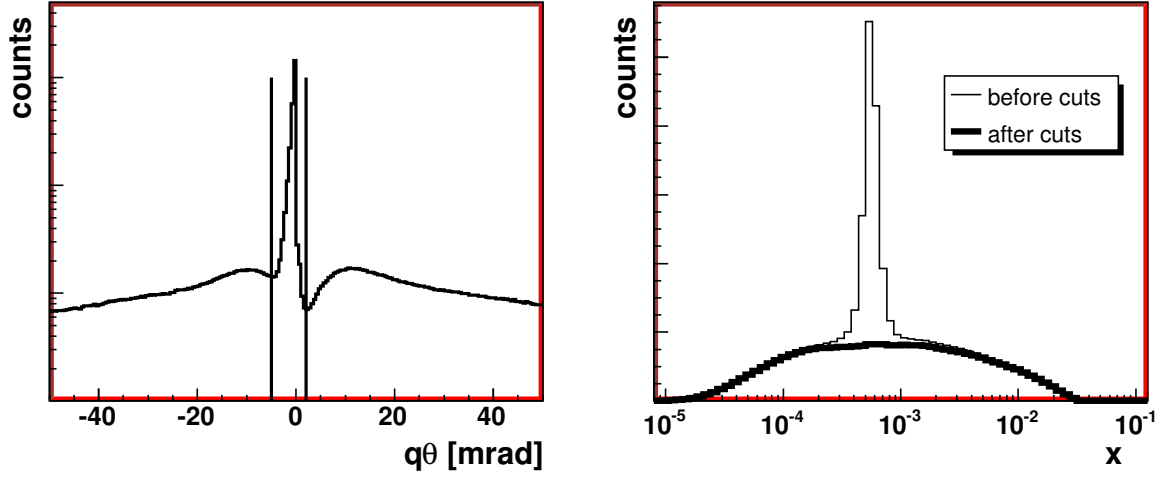
Figure 2: Removal of the $\mu^+ e^- \to \mu^+ e^-$ scattering events. **Left:** distribution of the variable $q\theta$ (see text for the definition) for events with one (positive or negative) hadron candidate outgoing from the primary interaction point. Events between vertical lines are removed from further analysis. Note the logarithmic scale on the vertical axis. **Right:** x distribution of events with one negative hadron candidate, before and after μe event rejection.
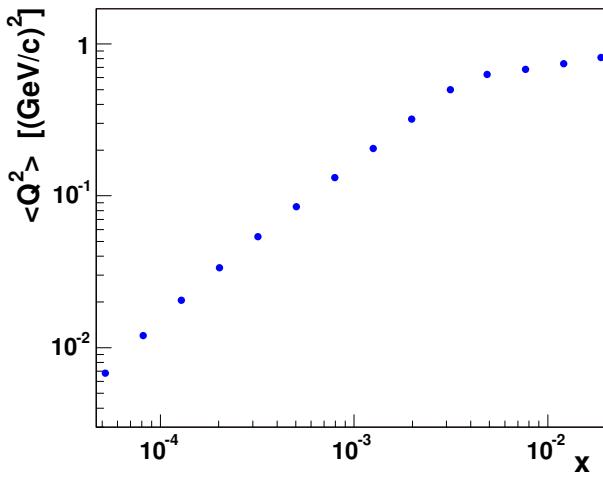
Figure 3: $\langle Q^2 \rangle$ as a function of x for the final data sample.
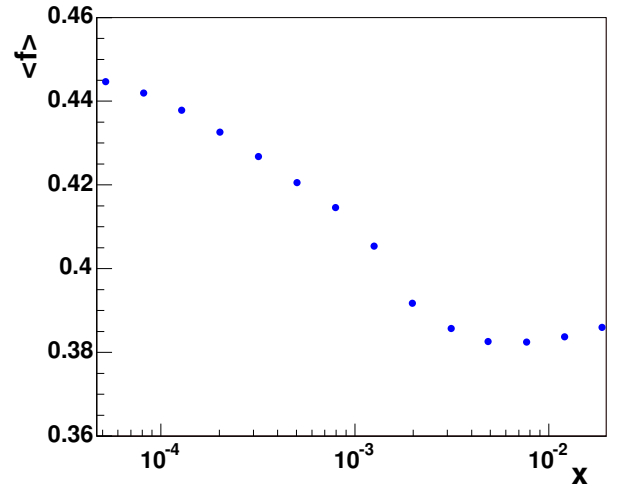
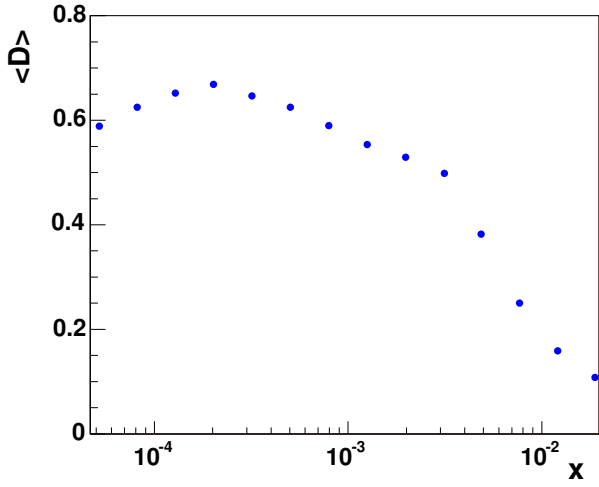Figure 4: Mean effective dilution factor, $\langle f \rangle$, as a function of x for the final data sample.
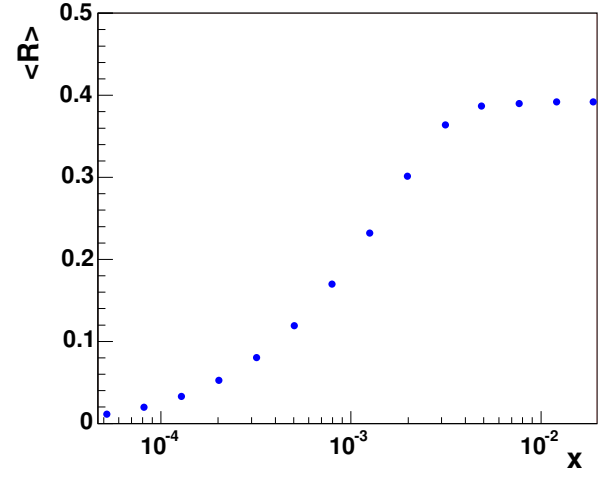
Figure 5: Mean depolarisation factor, $\langle D \rangle$, as a function of x for the final data sample.

Figure 6: Mean values of the ratio $R = \sigma^L/\sigma^T$ as a function of x for the final data sample.
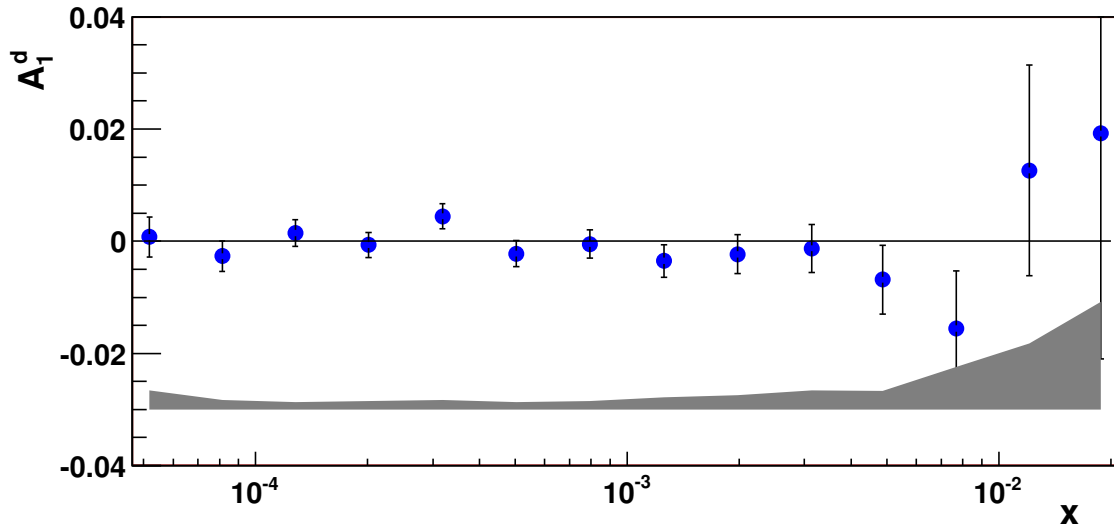

Figure 7: The asymmetry $A_1^d(x)$ as a function of x at the measured values of Q^2 obtained in this analysis. Errors are statistical; the shaded band indicates the size of the systematic ones.
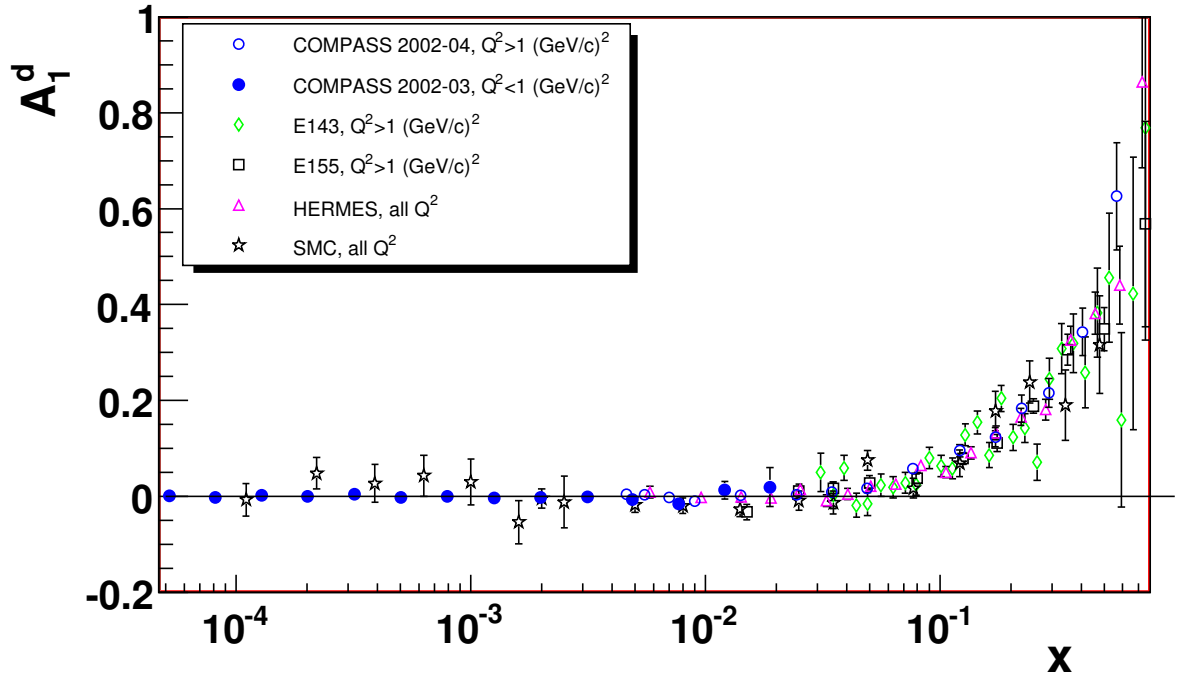
Figure 8: The asymmetry $A_1^d(x)$ as a function of x at the measured values of Q^2: the results for $Q^2 < 1 \ (\mathrm{GeV}/c)^2$ obtained in this analysis are compared with previous results at different values of Q^2 from COMPASS [12], SMC [8,13], HERMES [11], SLAC E143 [9] and SLAC E155 [10]. The E155 data correponding to the same x have been averaged over Q^2. Errors are statistical.
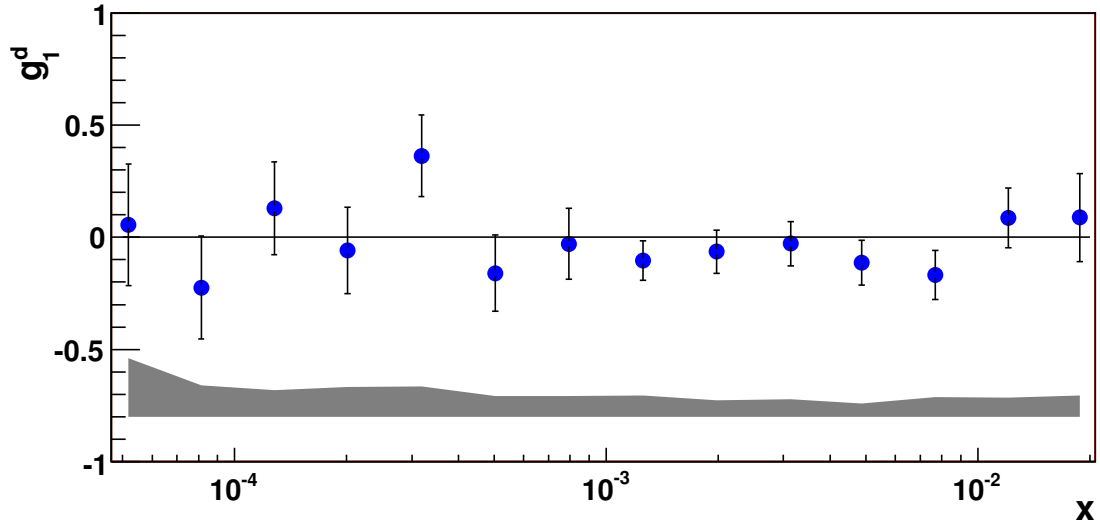

Figure 9: The spin dependent structure fnction $g_1^d(x)$ as a function of x at the measured values of Q^2 obtained in this analysis. Errors are statistical; the shaded band indicates the size of the systematic ones.
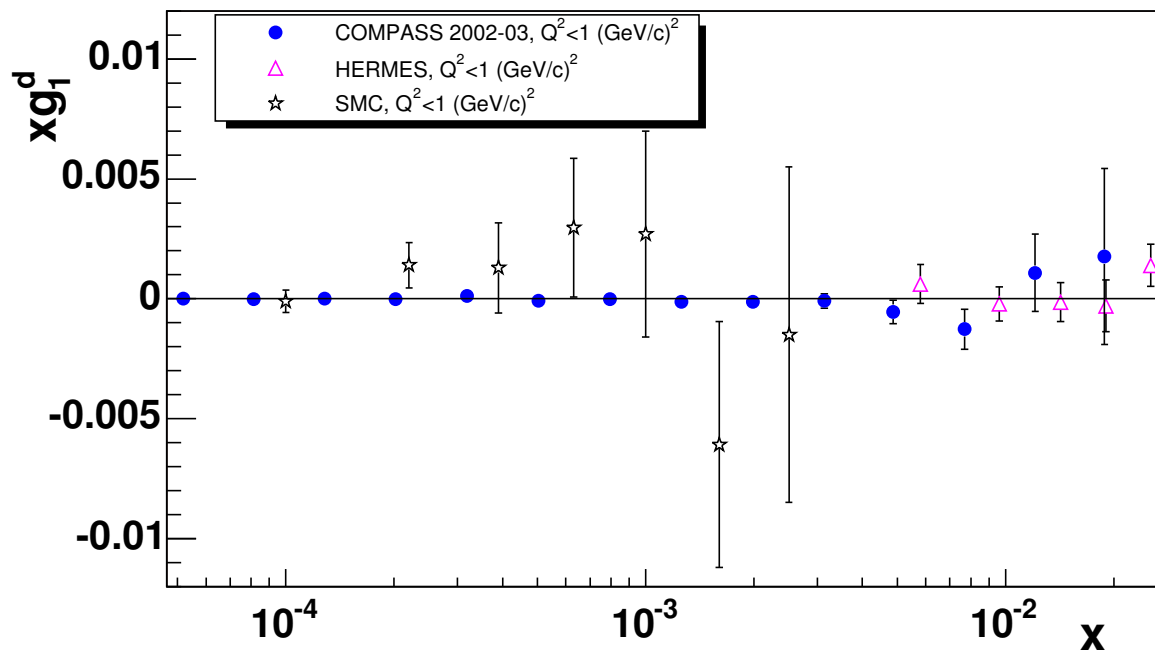
Figure 10: Same as in Fig. 8 but for the quantity xg_1^d. Only data for $Q^2 < 1$ $(\mathrm{GeV}/c)^2$ are shown.

14